



Experimental investigation of the two-phase local heat transfer coefficients for condensation of R134a in a micro-structured plate heat exchanger

Ru Wang¹ · Tingyan Sun¹ · Anja-Elsa Polzin¹ · Stephan Kabelac¹

Received: 16 November 2020 / Accepted: 21 May 2021 / Published online: 5 June 2021
© The Author(s) 2021

Abstract

Plate heat exchangers are widely used for two-phase heat transfer in the industrial applications, and recently more attention has been paid to the plate heat exchangers with enhanced surface due to their better heat transfer performance. In this paper, the local condensation heat transfer coefficients are studied using R134a in a micro-structured plate heat exchanger. In order to obtain a more accurate prediction model, a series of measurements are conducted under various operating conditions. The mass flux of R134a varied from 47 kg/m²s to 77 kg/m²s, the saturation pressure in the condenser ranged from 6.32 bar to 8.95 bar, and the value of the heat flux was between 13 kW/m² and 22 kW/m². The local two-phase Nusselt number increases with the increase of the mass flux. As the saturation pressure increases, the local two-phase Nusselt number increase at the beginning of the condensation and decrease at the end of the condensation. However, the effect of heat flux on local heat transfer is irregular, due to the interaction of these parameters in the experiment. Comparing with the unstructured plate heat exchanger, R134a condenses faster at the beginning of the process in the micro-structured plate heat exchanger, and the local heat transfer performs better when the vapor quality is lower. Combining with the phenomenon that the overall heat flux in micro-structured plate is larger under the same working conditions, it shows that the overall heat transfer of the micro-structured plate is improved, but the local heat transfer upgrades only at lower vapor qualities. A new correlation is developed, it predicts all the experimental data within the root mean square error 10%, and a new correlation for the waterside is suggested as well.

Keywords Local heat transfer coefficient · Condensation · Micro-structured · Plate heat exchanger

Abbreviations

A	Area (m ²)	G	Mass flux (kg/m ² s)
\hat{a}	Amplitude (m)	h	Enthalpie (J/kg)
B	Width (m)	L	Length (m)
c_p	Isobaric specific heat capacity (J/kg K)	\dot{m}	Mass flow (kg/s)
d	Diameter (m)	p	Pressure (Pa)
d_h	Hydraulic diameter (m)	\dot{Q}	Heat flow (W)
		\dot{q}	Heat flux (W/m ²)
		T	Temperature (K)
		x	Vapor quality
		Bo	Boiling number
		Co	Convection number
		Fr	Froude number
		Nu	Nusselt number
		Pr	Prandtl number
		Re	Reynolds number
		α	Heat transfer coefficient (W/m ² K)
		δ	Thickness (mm)
		η	Dynamic viscosity (Pa·s)
		Λ	Wavelength of plate (mm)

✉ Ru Wang
wang@ift.uni-hannover.de

Tingyan Sun
tysun1025@gmail.com

Anja-Elsa Polzin
polzin@ift.uni-hannover.de

Stephan Kabelac
kabelac@ift.uni-hannover.de

¹ Institute for Thermodynamics, Leibniz University Hannover,
30823 Garbsen, Germany

φ	Chevron angle of plate ($^{\circ}$)
λ	Thermal conductivity (W/mK)
ξ	Pressure drop factor
ψ	Area enlargement factor
ϕ	Two phase multiplier
acc	Acceleration
cal	Calculation
con	Condensation area
exp	Experiment
fric	Friction
g	Gravity
het	Heterogenic model
hom	Homogenies model
i	Number of lcal position, $i = 1 \sim 9$
j	Number of segment, $j = 1 \sim 8$
l	Liquid phase
m	Mean
man	Manifold
out	Outlet
r	Refrigerant
sat	Saturation
sp	Single phase
sub	Subcooling area
sup	Overheated area
tot	Total
tp	Two phase
v	Vapor phase
w	Waterside

1 Introduction

Plate heat exchangers (PHEs) have been widely used for industrial single-phase liquid-to-liquid heat transfer applications, such as pharmaceutical industry and chemical processing, due to their good thermal performance, modest space requirement, easy accessibility to all areas, lower capital and operating costs as compared to shell-and-tube heat exchangers. In the last 30 years, PHEs have also been increasingly used for two-phase heat transfer, particularly as evaporators and condensers in chillers and heat pumps as well as in process engineering systems [1]. Therefore, the heat transfer performance on condensation for different refrigerants in the PHEs has been intensively researched experimentally. Yan et al. [2] measured the heat transfer coefficient of condensation and frictional pressure drop of R134a in a vertical PHE. The results showed that the heat transfer coefficient and pressure drop normally increase with the mass flux, a corresponding correlation was also proposed. Jokar et al. [3] studied the heat transfer coefficient and pressure drop during condensation of R134a using two brazed PHEs, empirical correlations for this type of PHEs were developed, plotted and compared with relevant published results.

Garcia-Cascales et al. [4] carried out a set of evaporation and condensation tests, in which R22 and R290 were used as the working fluids for condensation. The results were compared with the correlations of Yan et al. [2], Kuo et al. [5], Han et al. [6], Thonon and Bontemps [7] and the modified correlation of Shah [8]. Mancin et al. [9] developed a computational procedure for heat transfer on condensation in PHEs, which was combined with gravity dominated and shear controlled condensation. The model was further validated by the experimental data from three PHEs with varied geometrical characters. Longo and his co-workers conducted a great deal of experiment on condensation heat transfer in brazed PHE with diverse refrigerants, namely R134a [10, 11], R410a [12], isobutene, propane and propene [13], R236fa [14], R1234yf [15], R1234ze [16] and R152a [17]. A detailed review of earlier research work and a discussion on the thermal–hydraulic performance of condensation in PHEs can be found in the book by Wang et al. [18]. A survey of correlations for heat transfer and pressure drop for condensation in PHEs is given by Eldeeb et al. [19]. Recently, Tao and Ferreira [20] assess eight heat transfer correlations and six frictional pressure drop correlations for condensation in PHEs with the database. They found that the correlation from Longo et al. [21] matches well with most available measurement data, they also developed a new correlation for friction pressure drop using multi-variable regression analysis with non-dimensional numbers, which predicted 87.5% of the available experimental data within 50%.

In order to improve the heat transfer performance further, the PHEs with an enhanced surface have been a topic of research in recent years. However, conventional methods such as the further development of embossing geometries and materials in PHEs are now reaching their limits in terms of their improvement potential. A new approach is the targeted development of surfaces, the properties of which favor the phase change on both a macroscopic and microscopic level. The advancing development of manufacturing processes in the nano- and microscale area enables an increasingly sophisticated integration of microstructures on technical surfaces. Many researches prove that these microstructures are not just about increasing the heat transfer area, they ensure a greater promotion in heat transfer with a small pressure drop penalty [1]. During condensation, there is often an uneven wettability of the surface in two-phase flow region, but poor wetting is required to maintain the droplet condensation, the drainage of the condensate can be more likely to result in well-wetting areas, therefore, microstructure is advantageous to improve this imbalance, it has a major influence on the formation of drops and help maintain droplet condensation for longer. In addition, the microstructure also influences other relevant mechanisms in heat transfer. The surface force is the main influence for characteristic lengths in

the range of capillary lengths, as is the case with microstructures, it can lead to deviating flow patterns such as an earlier onset of plug flow [22]. Different processes are used to produce microstructures on technical surfaces, such as sandblasting, coating, lithographic process and laser structuring. In general, two types of microstructures are used within for two-phase heat transfer so far: the crossed-grooved and the grooved microstructure [1]. Nilpueng and Wongwises [23] compared the heat transfer coefficient and pressure drop of water flow inside a PHE with a rough surface and another one with a smooth surface. It was found that the growth in surface roughness yielded an increase in heat transfer coefficient between 4.5% and 18% and an increase in pressure drop between 3.9% and 19.2% with respect to a smooth surface. Longo et al. [1] presented an experimental work using a crossed-grooved surface to study the evaporation and condensation inside the PHE. It indicated that the crossed-grooved surface gave a rise in the heat transfer coefficient from 30 to 40% in evaporation and up to 60% in condensation compared to the smooth surface PHE.

In this work, a series of measurements are conducted at the Institute for Thermodynamics, Leibniz University Hannover, where a PHE with micro pits is applied as a condenser to measure the two-phase local heat transfer coefficient of R134a. After data reduction, the influence of mass flow, saturation pressure and heat flux on the two-phase local heat transfer will be investigated, and the heat transfer performance will be compared with data from the unstructured PHE measured in previous work in the Institute [24]. As a result, a new correlation to determine the two-phase local heat transfer coefficient will be presented.

2 Experimental setup

The experimental system, seen and sketched in Fig. 1, consists of two main loops: the refrigerant loop and the secondary fluid loop. In this work, the refrigerant is R134a, the reason for selecting this refrigerant is that it has already been widely studied by a lot of researchers, a large amount of data can be used for comparison and analysis in this work. The

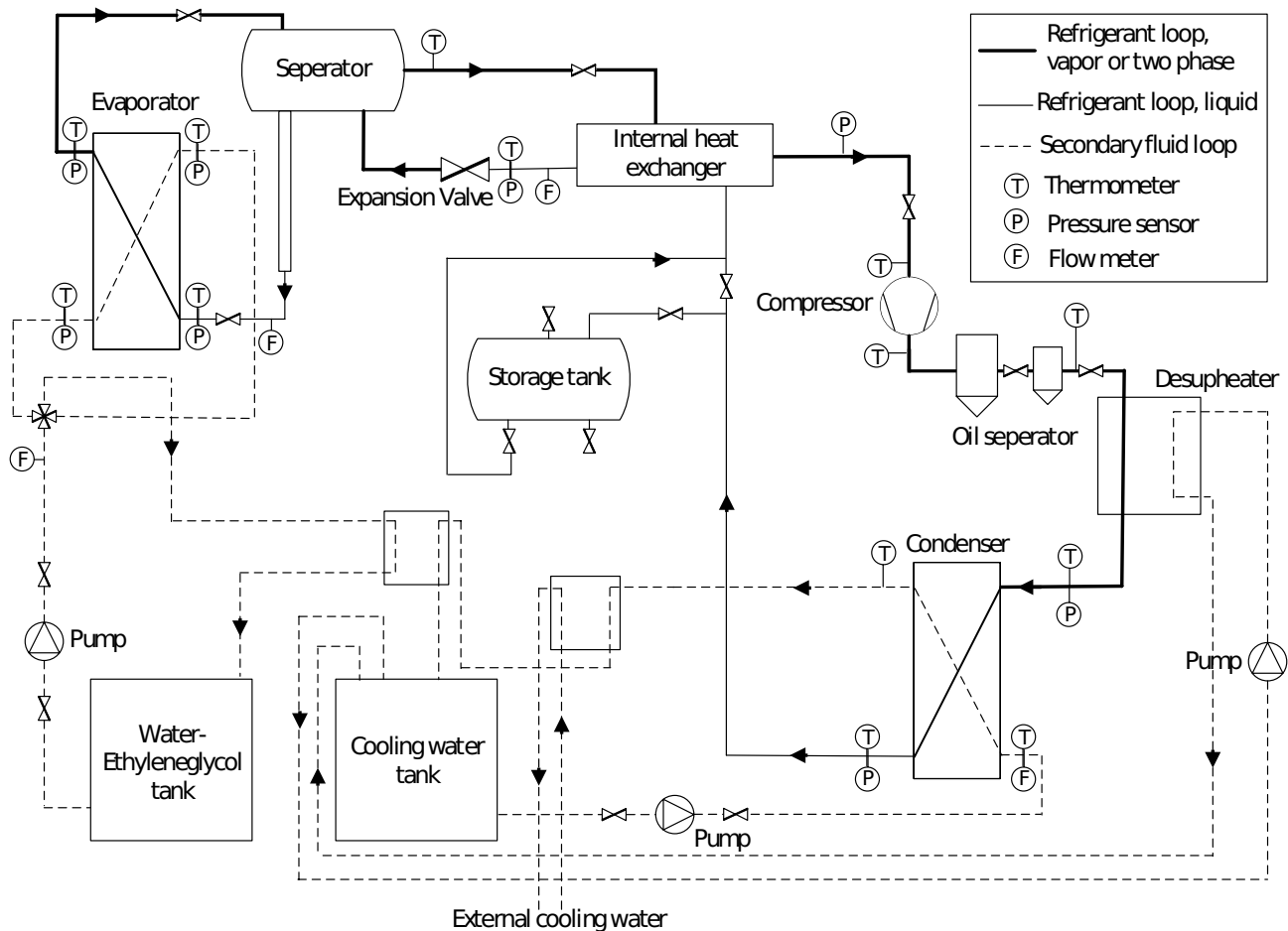


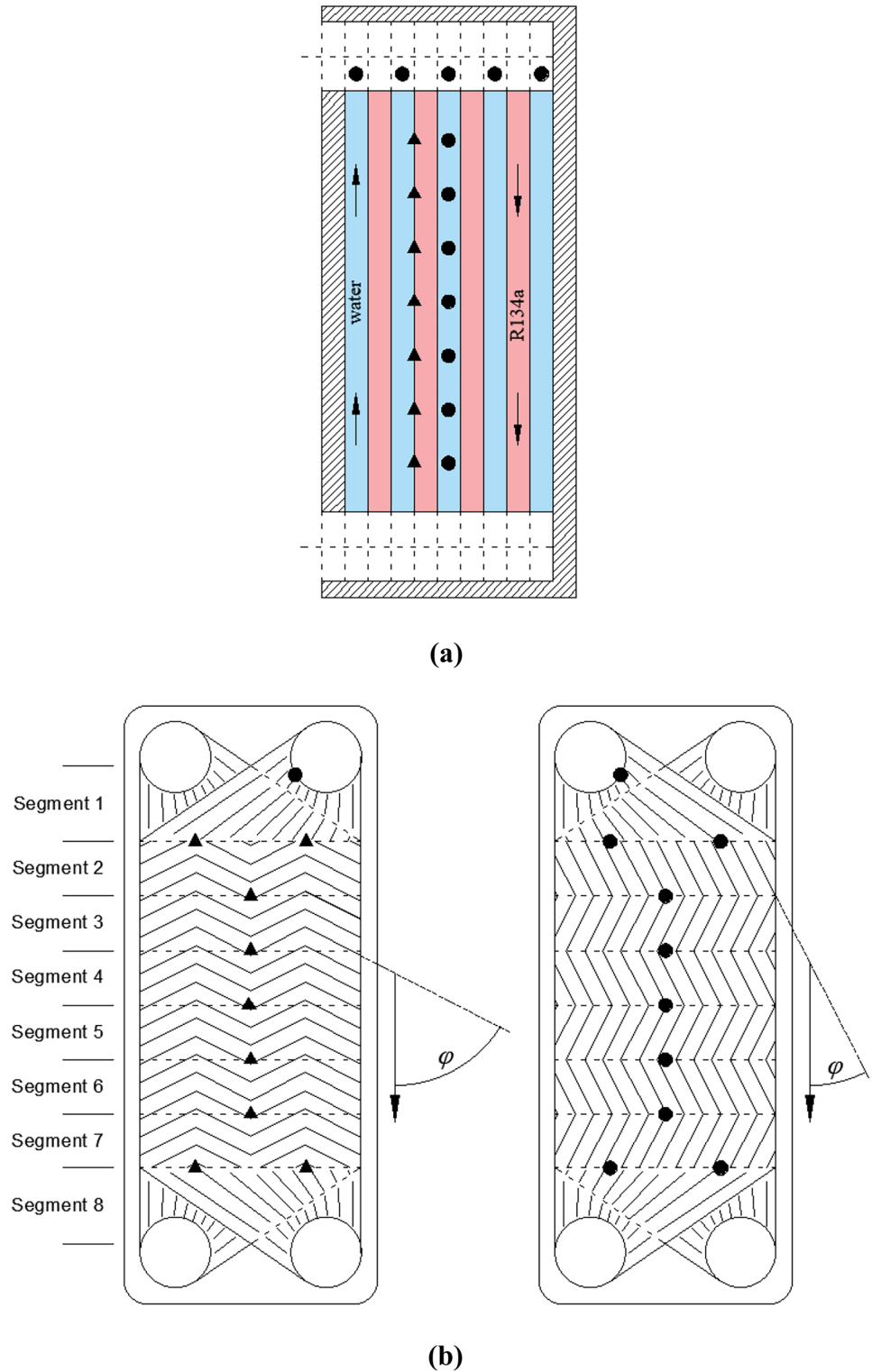
Fig. 1 Schematic diagram of experimental setup

secondary fluids are water and water-ethyleneglycol mixture in condenser and evaporator, respectively.

In the refrigerant loop, the liquid R134a having high pressure is led through an expansion valve. After partial evaporation the two-phase R134a enters into a separator where liquid and vapor are separated. Low pressure liquid flows

into the evaporator, in which R134a is heated by the water-ethyleneglycol mixture. The evaporator can be operated as a convectional natural cycle in a flooded, gravity driven thermosyphon mode or as a forced convection cycle using a magnetic driven pump. By switching the cycle mode the refrigerant loop can be controlled in a wide range on behalf

Fig. 2 (a) Configuration of the condenser plates; (b) Location of the thermocouples for local water (round icons) and wall (triangle icons) temperature



of the mass flux, which is measured with a Krohne ultrasonic flow meter. The two-phase flow exiting from evaporator is again separated in the separator. In order to obtain an over-heating, the saturated vapor from the separator is heated by the R134a liquid coming from the condenser by means of an internal heat exchanger. After flowing into a compressor, the overheated low-pressure R134a vapor becomes not only high-pressure but also highly superheated vapor. The compressor is a piston type F16/2051 compressor with 55 kW electric power max, provided by GEA Bock GmbH, to which two oil separators are connected to help returning the oil that enters the circuit during compression. The vapor then circulates through a desuperheater, in which the vapors is reduced to about 2 K superheated. The vapor is condensed by the cooling water in a PHE with micro pits on the plates. Two sight-glasses are located at the inlet and outlet of the condenser, respectively. The state of R134a at the outlet of the condenser is controlled to be liquid by adjusting the opening of the expansion valve and flow rate of the cooling water, thus the degree of subcooling at the outlet is about 1–2 K. In the second fluid loop the cooling water is pumped from a tank, and heated within the condenser. The water is cooled back down by external cooling water first, then it exchanges heat with the water-ethyleneglycol mixture that is used as the heating medium in the evaporator. PT100 resistant thermometers are used at the temperature measuring points shown in Fig. 1, the absolute pressures and pressure difference are measured by piezoresistive sensors. Flow rate of the secondary fluids are measured by electromagnetic flowmeters.

The condenser to be tested is a countercurrent industrial PHE with micro pits on Titanium plates provided by the EcoFlex series by Kelvion PHE GmbH. It consists of 4 refrigerant channels and 5 secondary fluid channels formed by 10 plates as shown in Fig. 2(a). The plates with two different chevron angles are arranged alternately, the secondary fluid temperature (round icons) and wall temperature (triangle icons) are measured with K-type thermocouples

in order to determine quasi local heat transfer coefficient. The thermocouples are located on the water side (round icons) along the plate as shown in Fig. 2(b), those for wall temperatures (triangle icons) are arranged on the adjacent water channel in order to avoid interference of too many thermocouples. The temperature profile of these two water channel is considered equal. Table 1 lists the accuracy of the sensors, the uncertainty of temperature and pressure sensors is related to measured value based on the calibration, while the uncertainty of flow meter is related to full scale.

The geometry of the plate is given in Fig. 3, and its geometrical parameters are listed in Table 2. Microstructures, which are micro pits in our case, are produced by using a rolling process on the plate surface. The microstructure is applied to the plate using a specially treated roller press. This procedure is done before another press creates the corrugated wave structure. The roller acts like a stamp and presses the microstructure homogeneously into the material, the resulting structure consists of oval elevations with a height of about 25 μm (as shown in Fig. 4), the detailed information refers to the work by Polzin et al. [24]. This concave microstructure is mainly designed for evaporators. In this work, it is used to study its effect on condensation. In addition, since the surface of the plate is not attacked as with a laser or an electrode treatment, this method avoids the problem of detaching micrometer-sized particles from the surface of the plate. For the secondary fluid side, there is no microstructure.

For the local temperature measurement, the head of the thermocouples are bended into the mainstream of the fluid channel, and the wire is welded on the plate a few millimeters below the head. Due to the titanium material (grade 1, material No. 3.7025), direct soldering of the thermocouples is not possible. Titanium always forms a thin oxide layer in an air atmosphere, which must be removed so that the solder can bond with the titanium. After removing the oxide layer, a coating with copper, silver or nickel is

Table 1 Accuracy of sensors related to condenser

Sensor	Type	Uncertainty	Range
Temperature	PT-100	± 0.04 K	-50 – 250 °C
Temperature	K-type	± 0.061 K	-200 – 1300 °C
Absolute pressure at inlet	Piezo resistive (IMP 321, ICS Schneider), stainless steel membrane	± 74 Pa	0 – 15 bar
Absolute pressure at outlet	Piezo resistive (DMU1, Afriso), thick-film ceramic measuring cell	± 74 Pa	0 – 15 bar
Differential pressure	2-piezoresistive (IDM 331), stainless steel membrane	± 21 Pa	-1 – 1 bar
Mass flow of R134a	Turbine (Model HM 013 E, KEM Küppers)	$\pm 0.1\%$	0.3–500 l/min
Mass flow of water	Electromagnetic (Proline Promag 53P, Endress & Hauser)	$\pm 0.2\%$	0 – 9600 m ³ /h
Mass flow of water	Electromagnetic (Proline Promag 53P, Endress & Hauser)	$\pm 0.2\%$	0 – 9600 m ³ /h

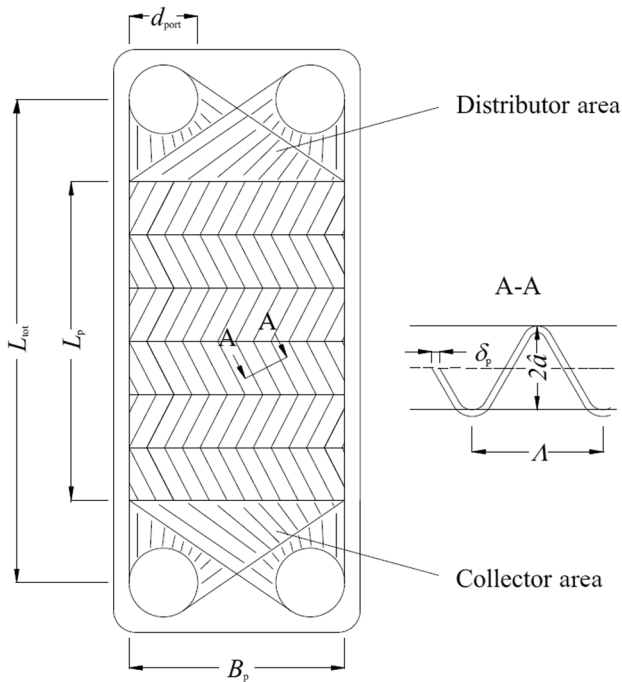


Fig. 3 Geometry of micro-structured plate

recommended, which prevents the surface from oxidizing again and significantly improves wettability and adhesion [25]. Therefore, in this work, a special soldering technique is used, that is, a layer of nickel coating is applied selectively to the desired positions by thermal spraying. For the wall temperature, the thermocouples are contacted with the plates by soldering them on the smooth surface, and fixed in the same horizontal position of the thermocouples for the secondary fluid. Because the uneven temperature distribution at the entry or exit of the triangle regions, i.e. the distributor and collector (seen in Fig. 3), two thermocouples are assigned to acquire meaningful local temperatures and to detect possible maldistribution.

Table 2 Geometrical parameters of PHE

Total length L_{tot}	1.09 m
Length of plate without triple area L_p	0.72 m
Width of plate B_p	0.486 m
Chevron angle of plate φ	$(27^\circ + 63^\circ)/2$
Diameter of port d_{port}	0.155 m
Amplitude \hat{a}	1.6 mm
Plate thickness δ_p	0.6 mm
Thermal conductivity of plate λ_p	21 W/m K
Wavelength of plate Λ	12 mm
Hydraulic diameter d_h	5.5 mm
Area enlargement factor ψ	1.159

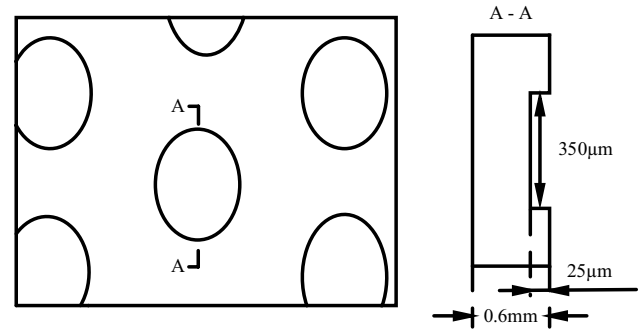


Fig. 4 Schematic diagram of micro structures on the plate

3 Data reduction

The calculation process for the heat transfer coefficient is based on the following assumptions: (1) Bassiouny model [26] is used to determine the mass flow distribution over the gap; (2) the heat loss on the outer surface of the condenser is negligible, because the saturation temperature of R134a in the test section is not much different from the ambient temperature. In order to calculate local heat transfer coefficient, the plate is divided into 8 segments according to the positions of the thermocouples as shown in Fig. 2b.

In segment j , as shown in Fig. 5, the local heat flux is determined by the mass flow of water and the measured local temperatures, it is assumed that the heat transferred by the water is equally divided between the front plate and the rear plate:

$$\dot{Q}_j = \dot{m}_w c_{p,w} (T_{w,i} - T_{w,i+1}) \tag{1}$$

$$\dot{q}_j = \frac{\dot{Q}_j}{2A_j} \tag{2}$$

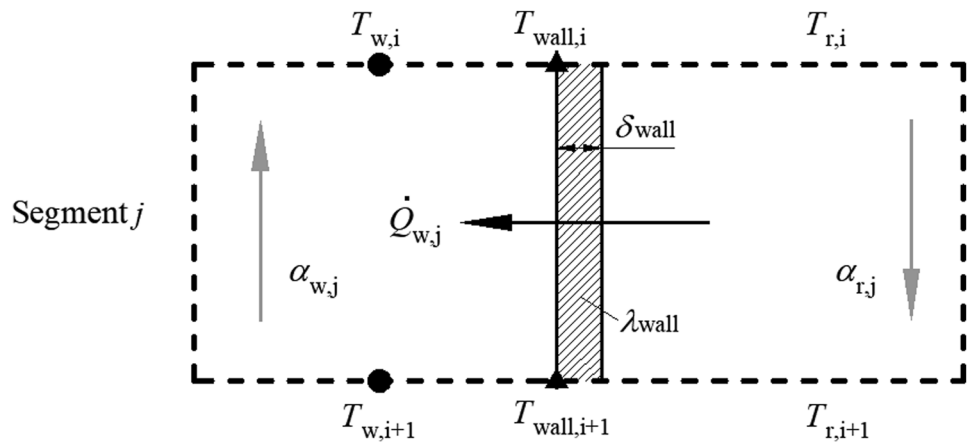
$$A_j = \frac{L_p}{6} B_p \psi \tag{3}$$

According to the energy balance between R134a and the cooling water, the enthalpy of the refrigerant R134a at position $i + 1$ is determined in the stationary case by:

Table 3 Assessment of the thermodynamic state in a segment

Condition	State of segment j
$h_{r,i} > h'_{r,i}, h_{r,i+1} > h'_{r,i+1}$	Overheated
$h_{r,i} \geq h'_{r,i}, h_{r,i+1} \leq h'_{r,i+1}$	Overheated and condensation
$h_{r,i} \leq h'_{r,i}, h_{r,i+1} \geq h'_{r,i+1}$	Condensation
$h_{r,i} \geq h'_{r,i}, h_{r,i+1} \leq h'_{r,i+1}$	Condensation and subcooled
$h_{r,i} < h'_{r,i}, h_{r,i+1} < h'_{r,i+1}$	Subcooled

Fig. 5 Schematic diagram of heat transfer process in segment j



$$h_{r,i+1} = h_{r,i} - \frac{\dot{Q}_j}{\dot{m}_r} \tag{4}$$

$$x_i = \frac{h_{r,i} - h'_{r,i}}{h''_{r,i} - h'_{r,i}} \tag{5}$$

Thus the temperature of R134a at position i $T_{r,i}$ can be obtained combining with the calculation of local pressure described in Eq. (17, 18).

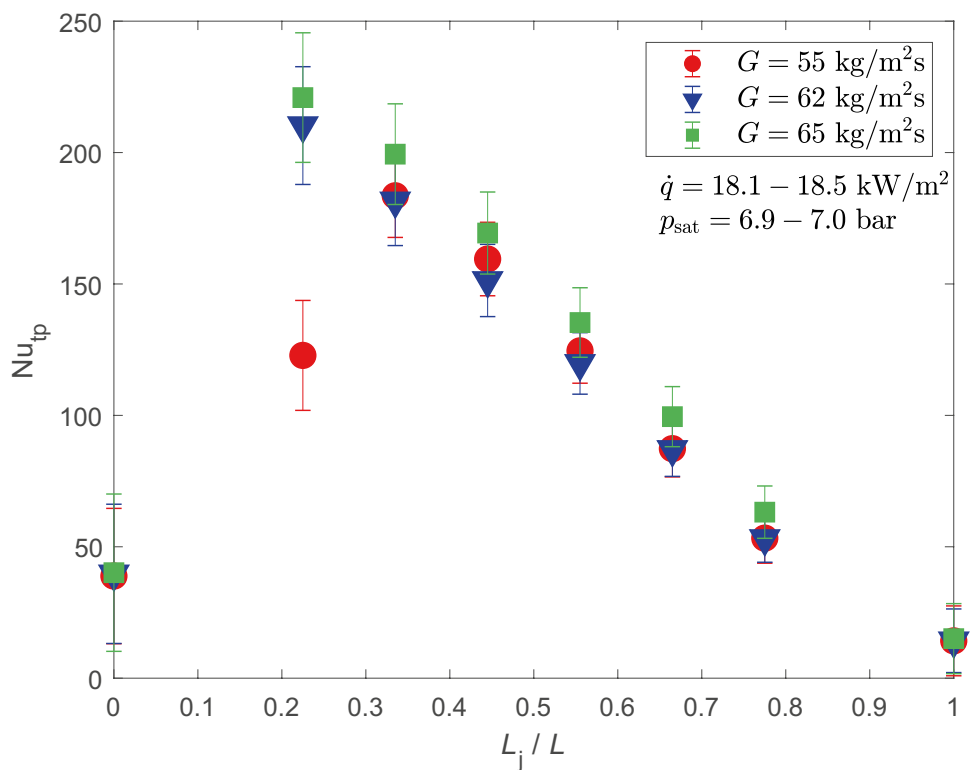
By comparing the calculated enthalpy with the saturation enthalpy at the same temperature or pressure, the thermodynamic state of R134a in each segment is listed as shown in Table 3. Moreover, the vapor quality of R134a at each position is calculated as follows:

where $h'_{r,i}$ and $h''_{r,i}$ refer to saturated enthalpies of liquid and vapor phase at position i , respectively. The length of the two-phase area, L_{con} , is determined by:

$$\dot{Q}_{supj} = \dot{m}_r (h_{r,1} - h^e_{r,i+1}) \tag{6}$$

$$L_{supj} = \frac{\dot{Q}_{supj}}{\dot{Q}_j} L_j \tag{7}$$

Fig. 6 Influence of mass flux on the two-phase local Nusselt number



$$\dot{Q}_{sub,j} = \dot{m}_r (h_{r,i} - h'_{r,i+1}) \quad (8)$$

$$L_{sub,j} = \frac{\dot{Q}_{sub,j}}{\dot{Q}_j} L_j \quad (9)$$

$$L_{con} = L_{tot} - \sum L_{sup,j} - \sum L_{sub,j} \quad (10)$$

where $L_{sup,j}$ and $L_{sub,j}$ are the length of the overheated area and subcooled area in segment j , respectively.

The local heat transfer coefficient for R134a and the cooling water are determined by the heat flux of segment j and the corresponding logarithmic mean temperature difference between the wall and the fluid:

$$\alpha_{w,j} = \frac{\dot{q}_j}{\Delta T_{w,j}} \quad (11)$$

$$\Delta T_{w,j} = \frac{(T_{wall,i+1} - T_{w,i+1}) - (T_{wall,i} - T_{w,i})}{\ln \frac{T_{wall,i+1} - T_{w,i+1}}{T_{wall,i} - T_{w,i}}} \quad (12)$$

$$\frac{1}{\alpha_{r,j}} + \frac{\delta_{wall}}{\lambda_{wall}} = \frac{\dot{q}_j}{\Delta T_{r,j}} \quad (13)$$

$$\Delta T_{r,j} = \frac{(T_{r,i+1} - T_{wall,i+1}) - (T_{r,i} - T_{wall,i})}{\ln \frac{T_{r,i+1} - T_{wall,i+1}}{T_{r,i} - T_{wall,i}}} \quad (14)$$

The pressure drop has an obvious influence on the heat transfer performance of condensation, it consists of four parts: acceleration pressure drop Δp_{acc} [27], gravity pressure drop Δp_g , the manifold pressure drop at the inlet and outlet Δp_{man} and the friction pressure drop Δp_{fric} . At the inlet and the outlet of the condenser, the manifold pressure drop occurs when the flow is deflected into each gap. It is calculated as following:

$$\Delta p_{man} = 1.4 \frac{G_{man}^2}{2\rho_{man}} \quad (15)$$

in which, the mass flux of R134a in the manifold G_{man} is calculated as Eq. (16).

$$G_{man} = \frac{\dot{m}_r}{A_{man}} \quad (16)$$

The area of the manifold A_{man} is equal to 0.019 m². For segment j , we have the overall pressure drop:

$$p_{r,i} - p_{r,i+1} = \Delta p_{acc,j} + \Delta p_{g,j} + \Delta p_{fric,j} \quad (17)$$

$$\Delta p_{acc,j} = -\frac{G_r^2 (x_{i+1} - x_i)}{\rho_{r,m,j}} \quad (18)$$

$$\Delta p_{g,j} = \rho_{r,m,j} g L_j \quad (19)$$

The mean density of R134a in segment j is calculated based on the homogeneous model:

$$\rho_{r,m,j} = \left(\frac{x_j}{\rho_{v,j}} + \frac{1-x_j}{\rho_{l,j}} \right) - 1 \quad (20)$$

x_j is the mean vapor quality of segment j , it is calculated as the arithmetic mean of x_i and x_{i+1} .

The friction pressure drop is created by the shear stress between the liquid and vapor as well as between the fluid and the wall. It must be calculated according to the status of the flow, i.e. the flow pattern. The Martin model [28] is used for a single-phase flow in the PHE, i.e., in the state of superheated or subcooled fluid:

$$\Delta p_{fric,sp,j} = \frac{\xi_{sp,j} G_r^2 L_j}{2d_h \rho_{r,m,j}} \quad (21)$$

Here the single-phase pressure drop coefficient $\xi_{sp,j}$ is relate to the chevron angle φ and Reynolds number Re :

$$\frac{1}{\sqrt{\xi_{sp,j}}} = \frac{\cos\varphi}{\sqrt{btan\varphi + c\sin\varphi + \frac{\xi_0}{\cos\varphi}}} + \frac{1 - \cos\varphi}{\sqrt{\xi_1}} \quad (22)$$

$$\xi_0 = \begin{cases} \frac{64}{Re_{sp,j}}, & Re_{sp,j} < 2000 \\ (1.8 \lg Re_{sp,j} - 1.5)^{-2}, & Re_{sp,j} \geq 2000 \end{cases} \quad (23)$$

$$\xi_1 = \begin{cases} a \left(\frac{597}{Re_{sp,j}} + 3.85 \right), & Re_{sp,j} < 2000 \\ a \left(\frac{39}{Re_{sp,j}^{0.289}} \right), & Re_{sp,j} \geq 2000 \end{cases} \quad (24)$$

where Re_{sp} is the Reynolds number of the single phase flow in segment j . It is calculated as:

$$Re_{sp,j} = \frac{G_r^2 (1-x_j) d_h}{\eta_{sp,j}} \quad (25)$$

The empirical constants a , b and c take different values under different experimental conditions and geometries of plates. Here we take $a=0.43$, $b=1.86$, $c=0.6$, which is found by adapting our data.

The Grabenstein model [29] is used for the two-phase flow. This model is composed of two parts: a homogeneous flow contribution and a heterogeneous flow contribution.

$$\Delta p_{\text{fric,tp},j} = (1 - x_j) \Delta p_{\text{fric,tp,hom},j} + x_j \Delta p_{\text{fric,tp,het},j} \quad (26)$$

The homogeneous model assumes that the flow velocities of the gas and liquid phase are approximately equal, thus there is no slip at the vapor–liquid phase boundary. The pressure drop using the homogeneous model is calculated as follows:

$$\Delta p_{\text{fric,tp,hom},j} = \frac{\xi_{\text{tp},j} G_r^2 L_j}{2d_h \rho_{r,m,j}} \quad (27)$$

where the two-phase pressure drop coefficient $\xi_{\text{tp},j}$ is defined as:

$$\xi_{\text{tp},j} = C_{\text{hom}} \text{Re}^{n_{\text{hom}}} \quad (28)$$

The heterogeneous model was developed by Lockhart and Martinelli [30], in which two phases are considered separately, and a factor ϕ_1 is introduced to calculate the friction pressure drop of the two-phase flow as compared to the liquid phase.

$$\Delta p_{\text{fric,tp,het},j} = x_j \phi_1^2 \Delta p_{\text{fric,l},j} \quad (29)$$

$$\phi_1 = 1 + \frac{C_{\text{het}}}{\sqrt{\frac{\Delta p_{\text{fric,l},j}}{\Delta p_{\text{fric,v},j}}}} \quad (30)$$

The friction pressure drop of the liquid phase $\Delta p_{\text{fric,l},j}$ and the vapor phase $\Delta p_{\text{fric,v},j}$ are calculated using Eq. (21), the empirical parameters C_{hom} , n_{hom} , and C_{het} are 255, -0.614 and 0.905, respectively.

Therefore, the friction pressure drop in segment j is:

$$\Delta p_{\text{fric},j} = \Delta p_{\text{fric,sp},j} + \Delta p_{\text{fric,tp},j} \quad (31)$$

After calculation of the friction pressure drop of the segment, the local pressure at each position along the entire plate is obtained. Thus, the calculated pressure at the outlet is attained. A MATLAB program is applied to solve the above equations until the preset accuracy is reached by comparing the calculated outlet pressure with the measured outlet pressure.

$$p_{\text{cal,out}} = p_{r,i=9} - \Delta p_{\text{man,out}} \quad (32)$$

$$\Delta p_{\text{man,out}} = 1.4 \frac{G_r}{2\rho_{r,\text{man,out}}} \quad (33)$$

$$\text{accuracy} = \frac{p_{\text{cal,out}} - p_{\text{exp,out}}}{p_{\text{exp,out}}} \quad (34)$$

In our previous work, through measurement, about 0.08–0.25% by weight of the working fluid is substances

other than R134a, such as oil from the compressor and other particles in fittings that are not made of stainless steel [24]. This weight is small and ignored in this work. Therefore, the thermal physical properties of oil-free refrigerant R134a and pure water involved in the above equations are acquired by the REFPROP program from NIST.

An uncertainty analysis was carried out according to Moffat [31] for the determination of two-phase local heat transfer coefficients. The results show that the uncertainty of the condensation heat transfer coefficients is approximately 15%.

4 Result and discussion

4.1 Effect of operating conditions

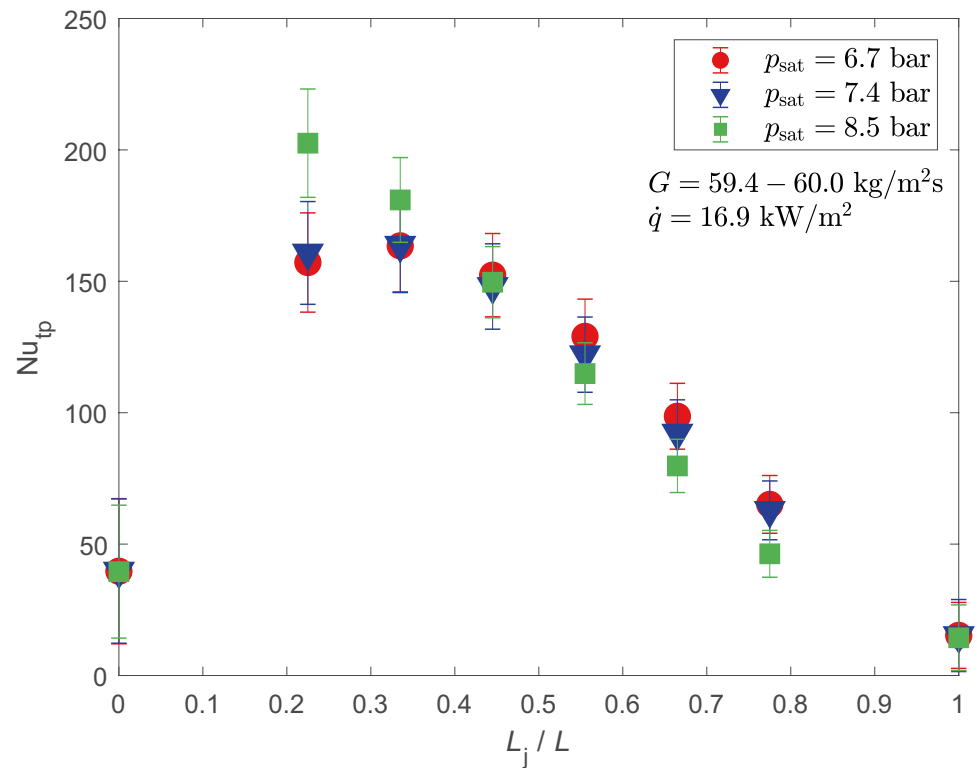
A series of experiments on the condensation of R134a in a micro-structured PHE was conducted under various working conditions. The mass flux of R134a varied from 47 kg/m²s to 77 kg/m²s, the saturation pressure in the condenser ranged from 6.32 bar to 8.95 bar, and the value of the heat flux was between 13 kW/m² and 22 kW/m².

Figure 6 reveals the influence of mass flux on the two-phase local Nusselt number Nu_{tp} at a heat flux of approximately 18 kW/m² and a saturation pressure of 7 bar, when the dimensionless length L_j/L is equal to 1 and 0, it represents the single-phase heat transfer of superheated vapor at the inlet and the subcooled liquid at the outlet, which are calculated by Martin correlation. When $L_j/L = 0.225$ and the mass flux is 55 kg/m²s, Nu_{tp} is much lower than other two groups, this is because there is large amount of superheated vapor in this segment, where the vapor quality is 0.935, R134a performs single-phase heat transfer first and then condensation starts. Overall, the increase in mass flux results in an increase in Nu_{tp} .

Figure 7 indicates Nu_{tp} at different saturation pressures. The heat transfer coefficients at the saturation pressures of 6.7, 7.4 and 8.5 bar are compared in the case of the same heat flux of 16.9 kW/m² and the same mass flux of 60 kg/m²s. Nu_{tp} increase with the increase of the saturation pressure when $L_j/L < 0.4$, this may be due to the fact that in this region, the higher temperature difference caused by the larger saturation pressure makes heat transfer significantly enhanced. However, when $L_j/L > 0.4$, the heat transfer enhancement caused by the high saturation pressure thickens the liquid film and increases the thermal resistance. When the hindrance of the liquid film is greater than the enhancement effect of the high saturation pressure, Nu_{tp} will decrease.

The variation of Nu_{tp} with the dimensionless length of the plate at the heat flux of 17.7, 18.2 and 19.3 kW/m²

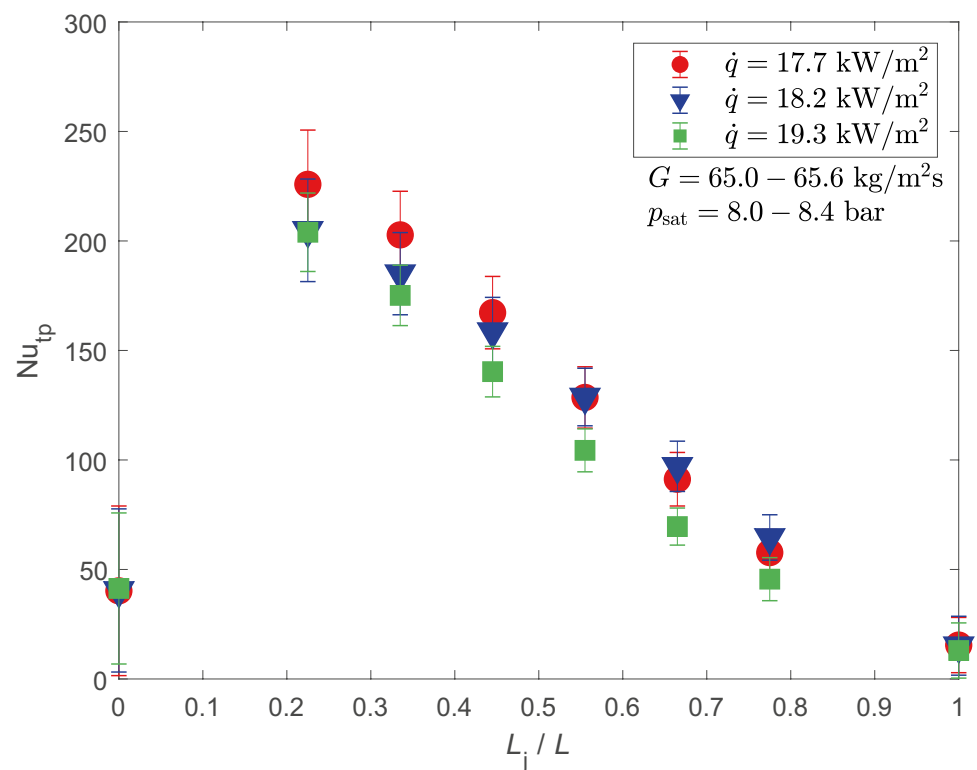
Fig. 7 Influence of saturation pressure on the two-phase local Nusselt number



are presented in Fig. 8, in which the mass flux is approx. $65 \text{ kg/m}^2\text{s}$ and the saturation pressure is approx. 8.2 bar . No simple trends can be seen there. If the vapor quality is more than 0.3 (dimensionless length is less than 0.6), Nu_{tp} decreases with the heat flux increasing. However, the

change is irregular at higher vapor qualities. The interaction of mass flux, saturation pressure and heat flux occurred during the measurement makes it difficult to change only one parameter and keep the other parameters constant. This means that when analyzing the effect of

Fig. 8 Influence of heat flux on the two-phase local Nusselt number



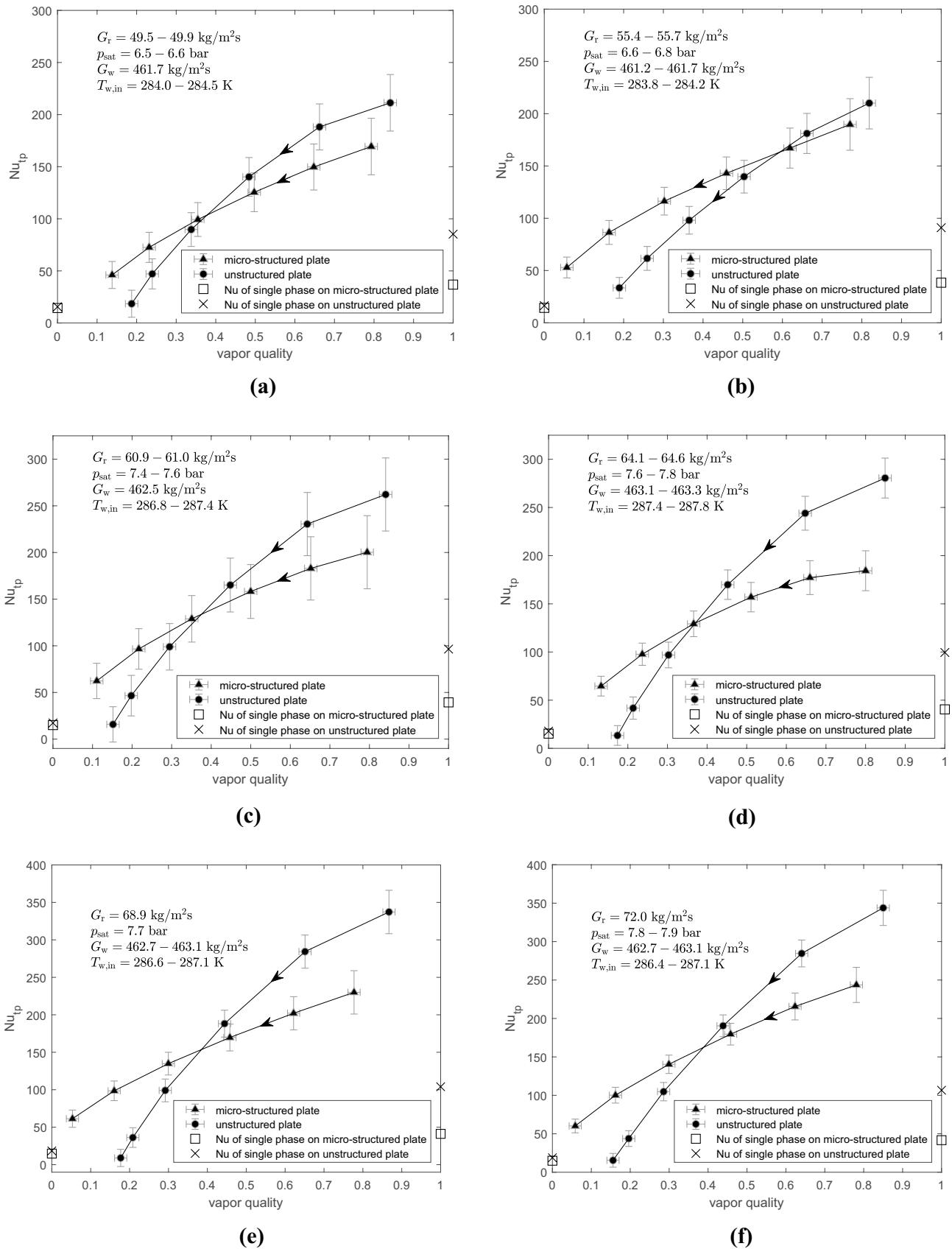


Fig. 9 Comparison of two-phase local Nu between the micro-structured plate and unstructured plate under six typical operating conditions

one parameter on the two-phase local heat transfer coefficient, the other two parameters float in a small range. This may lead to difficulties in drawing conclusions.

4.2 Comparison with unstructured plates

As mentioned in Sect. 1, the micro-structured plate enlarges the heat transfer area and can help to improve the formation of drops compared to the unstructured plate. Figure 9 shows six graphs of Nu_{tp} as a function of vapor quality for the micro-structured plate as compared to the “smooth” (unstructured) plate surface (as shown in Fig. 4(a)). The measurements with unstructured plate were conducted in our previous study [24]. Here, the mass flux of R134a and the cooling water, the saturation pressure and the inlet temperature of the cooling water are chosen to be as consistent as possible. On the one hand, it is clear that Nu_{tp} of these two types of plate increases significantly with the increase of vapor quality, it can be concluded that the enhancement of two-phase heat transfer occurs in the area where condensation starts, where the liquid film on the wall is thin, so the thermal resistance is small. On the other hand, the heat transfer performance of the micro-structured plate is worse than that of the unstructured plate when the vapor quality is higher, i.e., at the beginning of the condensation. In detail, Nu_{tp} for the micro-structured case is lower than that of the unstructured (smooth) case from a vapor quality of

approximately 0.38 for all the operating conditions studied in Fig. 9 except for case (b) where Nu_{tp} becomes lower from a vapor quality of 0.6. An explanation that can be given for this phenomenon is: at the beginning of condensation, the condensate liquid is filled into the depressions of the micro-structured plate due to its small amount. The condensate has a lower flow velocity there because of the pin obstacles and the resulting liquid film increases the thermal resistance. Therefore, the local heat transfer performance is impeded. Instead, when the vapor quality is lower, condensation heat transfer becomes the main mechanism, the additional liquid film formed by the pits could be negligible relative to the thickness of the entire liquid film, and the influence of laminar bottom layer is less compared with turbulent flow. Therefore, the micro-structured plate behaves better on behalf of two-phase local heat transfer at lower vapor qualities.

Besides, it can be seen that at the beginning of the condensation, since the temperature measurement of each segment is performed at the same position for the micro-structured plate and the unstructured plate, the vapor qualities of the micro-structured plate at the same position are lower compared with the unstructured plate. In other words, the vapor condenses faster on the micro-structured plate.

Figure 10 compares the overall heat flux of the six groups in Fig. 9. It is clear that the micro-structured plate acquires higher heat flux. It can be concluded that the micro-structured plate has a better overall heat transfer performance

Fig. 10 Comparison of heat flux between micro-structured plate and unstructured plate

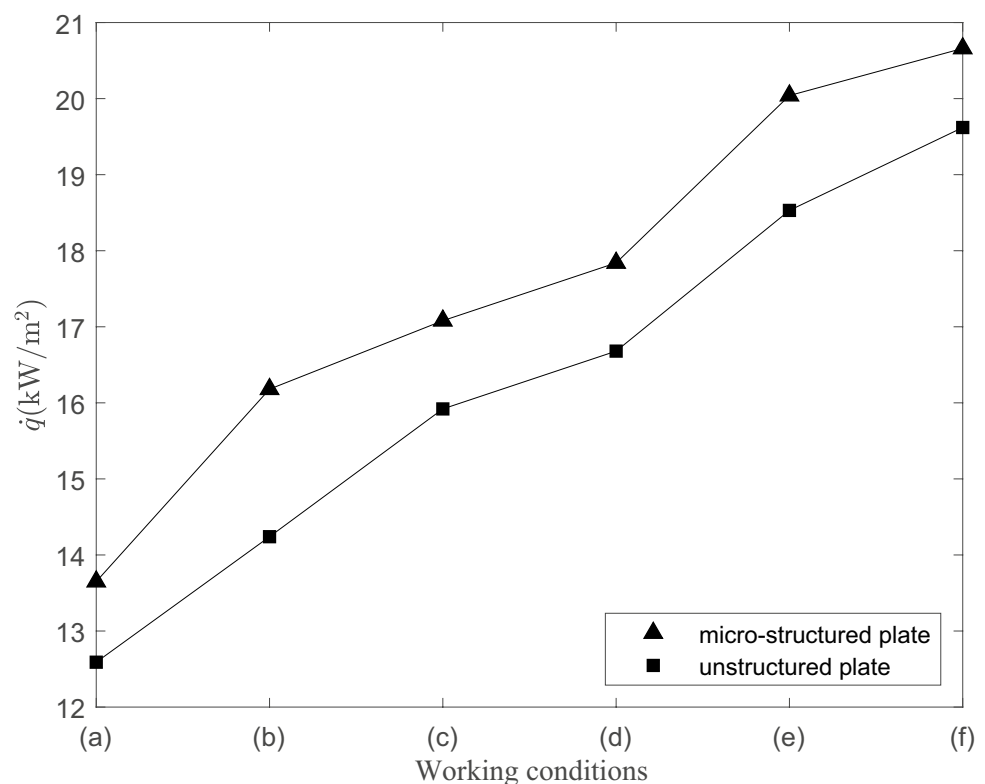


Table 4 Original correlations from the existing literatures and optimized forms

Author	Original correlation	Optimized correlation	RMSE
Yan et al. [2]	$Nu = 4.118Re_{eq}^{0.4}Pr_1^{1/3}$	$Nu = 0.00157Re_{eq}^{1.25}Pr_1^{1/3}$	25%
Kuo et al. [5]	$Nu = 0.2092Re_{lo}^{0.78}Pr_1^{1/3} \left(\frac{\eta_l}{\eta_{l,wall}} \right)^{0.14} \dots$ $\dots (0.25Co^{-0.45}Fr^{0.25} + 75Bo^{0.75})$	$Nu = 0.045Re_{lo}^{0.97}Pr_1^{1/3} \left(\frac{\eta_l}{\eta_{l,wall}} \right)^{1.7} \dots$ $\dots (0.076Co^{-0.68}Fr^{0.1} + 500Bo^{1.03})$	15%
Shah [8]	$Nu = 0.023Re_{lo}^{0.8}Pr_1^{0.4} \dots$ $\dots \left[(1-x)^{0.8} + \frac{3.8x^{0.76}(1-x)^{0.04}}{Pr^{0.38}} \right]$	$Nu = 0.002Re_{lo}^{1.22}Pr_1^{0.4} \dots$ $\dots \left[(1-x)^{0.038} + \frac{4.44x^{0.95}(1-x)^{0.15}}{Pr^{0.44}} \right]$	21%
Longo et al. [21]	$Nu = 1.875\phi Re_{eq}^{0.445}Pr_1^{1/3}$	$Nu = 0.0014\phi Re_{eq}^{1.25}Pr_1^{1/3}$	25%
Würfel and Ostrowski [32]	$Nu = 3.2Re_h^{0.46}Pr_1^{0.33}$	$Nu = 0.048Re_h^{0.7}Pr_1^{0.33}$	19%
Müller et al. [33]	$Nu = 0.15\sin\phi Re_{eq}^{0.5}Pr_1^{0.4}Bd^{0.6}p_r^{-0.2}\chi^{0.7}$	$Nu = \frac{1}{9523.8}\sin\phi Re_{eq}^{1.25}Pr_1^{0.4}Bd^{0.48}p_r^{-0.75}\chi^{0.00055}$	24%

under the same operating conditions in comparison with unstructured plates. Combining the phenomenon at the lower vapor quality shown in Fig. 9, it is seen that heat transfer performance of the plate with micro pits with only low vapor qualities is a function of vapor quality.

This experimental result is different from the results of the microstructure corrugated plate surface reported by Longo et al. [1]. They reported on a strong increase up to 60% in heat transfer for a crossed grooved surface, which is a convex structure that is different from the pits used in this work. Therefore,

the geometric type of the microstructure seems to be very important in that it has to match the wetting behavior of the fluid on the surface. This does not fit well in our situation.

4.3 A new correlation

Many researchers have described a variety of correlations of heat transfer coefficient in condensation in the literature. In this work, we compared the measured Nu_{tp} with the results of six correlation evaluations in the literature. In addition,

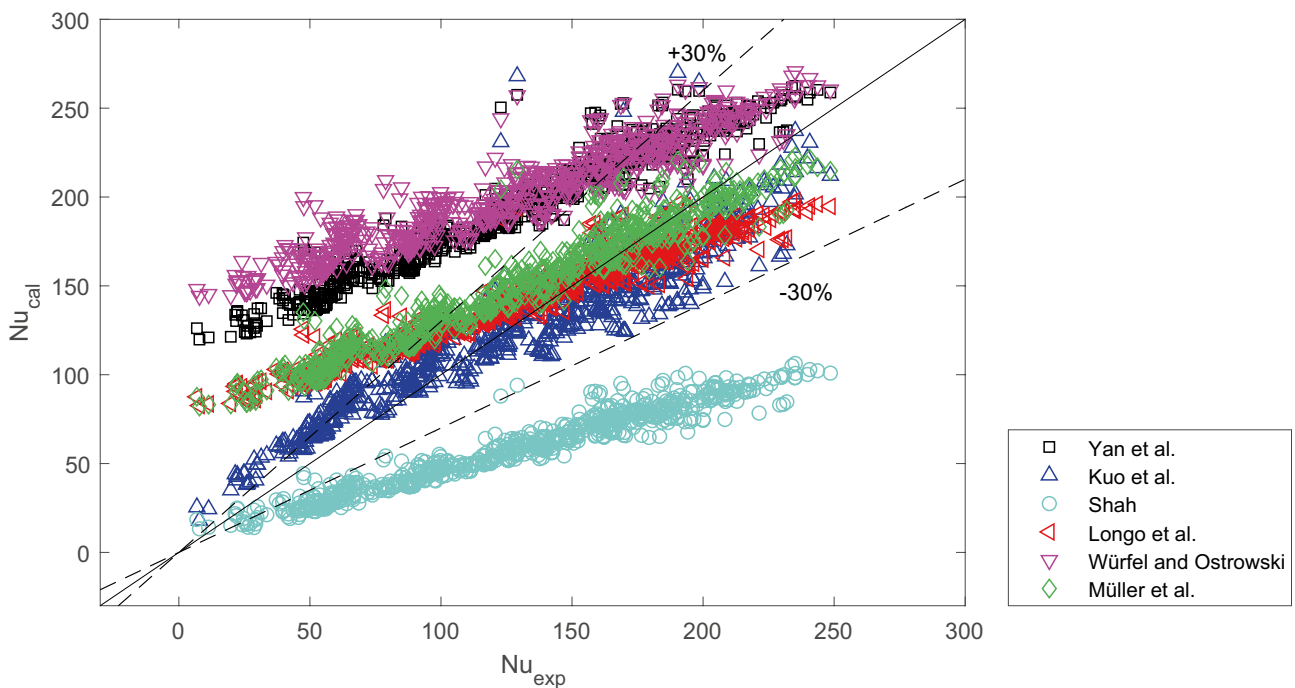


Fig. 11 Comparison of two-phase local Nu by selected correlations with experimental data

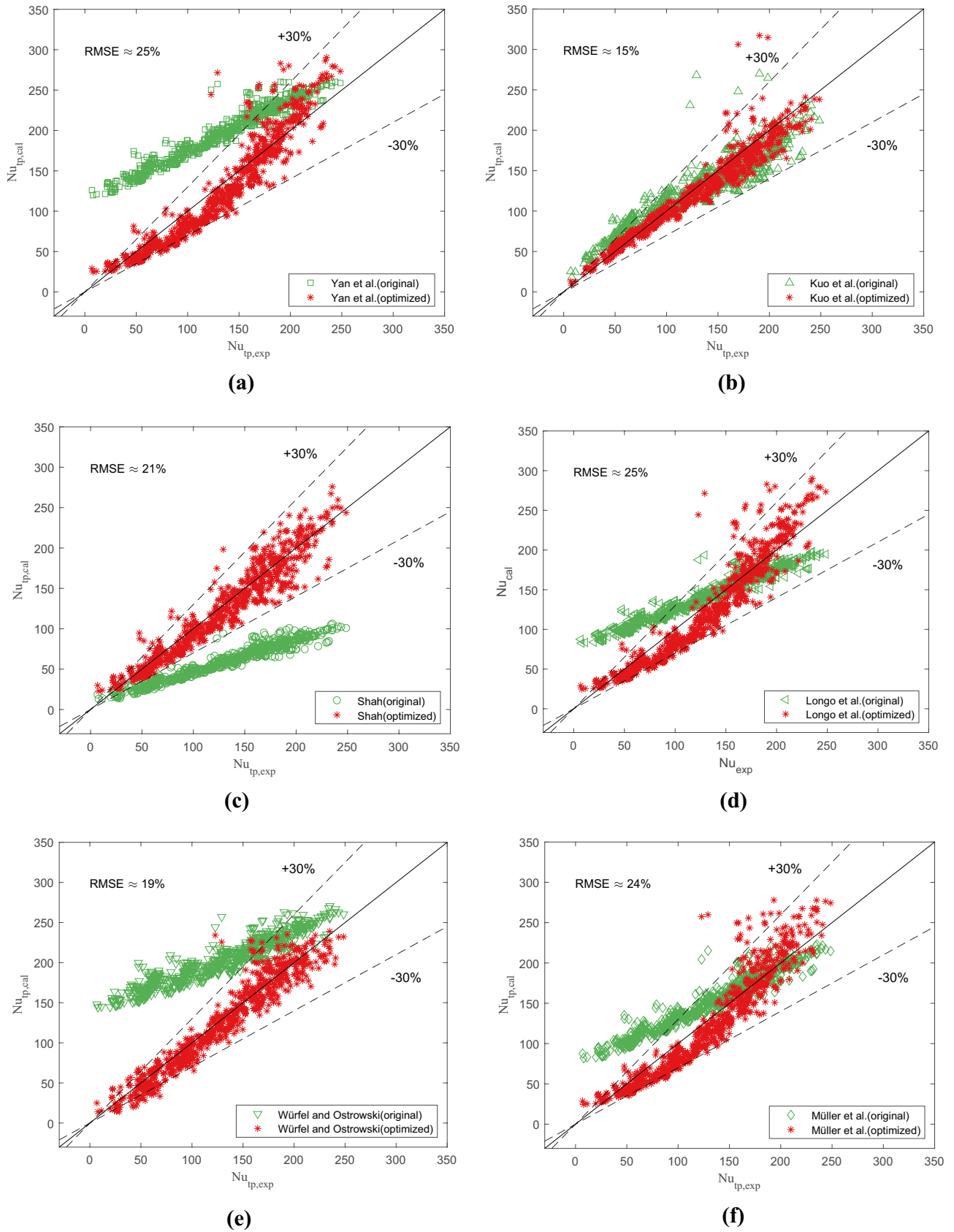


Fig. 12 Comparison of two-phase local Nu by optimized existing correlations with experimental data

a new correlation of the two-phase local heat transfer coefficient in the micro-structured PHE is derived after further analysis.

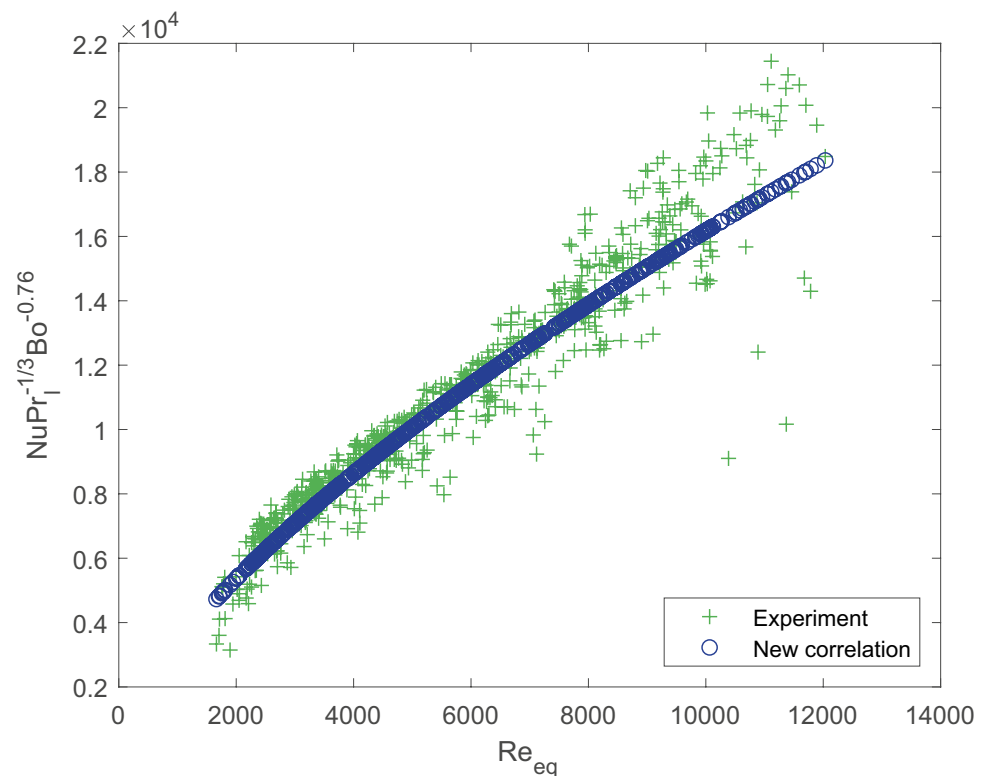
The correlations of Yan et al. [2], Kuo et al. [5], Shah [8], Longo et al. [21], Würfel and Ostrowski [32] and Müller et al. [33] of the type used clearly defined parameters to take $Nu = f(Re, Pr \dots)$ as a simple form and correlated them to their own experimental data. The equations are given in Table 4. Although Shah's correlation is theoretically derived from pipes, it is selected for comparison due to its wide applicability. Figure 11 presents a plot showing the comparison between the calculated Nu_{tp} using the 6 selected correlations and the measured Nu_{tp} . It indicates that the deviations between experimental values and calculated values for all the correlations involved are particularly large. In order to adapt the experimental data to the correlations, the constants and exponents in the correlations are modified by use of the particle swarm solver, which is an optimization function provided by MATLAB. The particle swarm optimization is a population-based stochastic algorithm. The search space is formed by setting the upper and lower limits of the variables to be modified. A particle is randomly selected as the initialization point from which the Root Mean Squared Error (RMSE) defined by Eq. (35) is temporarily determined as the optimal result. The next running particle circulates around the area centered on the best result. A lower value RMSE is determined as the new best result. Finally, the smallest RMSE and the corresponding optimal coefficients in a search space are obtained.

$$RMSE = \sqrt{\frac{\sum_n \left(\frac{a_{cal} - a_{exp}}{a_{exp}} \right)^2}{n}} \quad (35)$$

Figure 12 displays that the modification improves significantly the agreement between the experimental and calculated Nu_{tp} . All optimized correlation and their original forms are listed in Table 4. The correlation from Yan et al. [2] has the simplest structure, which is only a combination of the equivalent Reynolds number Re_{eq} and Prandtl number of liquid phase Pr_1 , but the RMSE is 25%. The optimized correlation from Kuo et al. [5] has the smallest RMSE (15%). However, the deviation of the three test points is larger than $\pm 30\%$ as shown in Fig. 12(b), because the segments represented by these points are still in a thermodynamic transition state from superheating to condensation. Therefore, these three abnormal points are ignored in the optimization procedure. Thus, the optimized correlation derived from Kuo et al. is quite good for all experimental data that are completely in the two-phase condensation region.

Furthermore, the correlation of Kuo et al. [5] reveals that in addition to Re_{eq} and Pr_1 , there are three other influencing parameters, namely convection number Co , Froude number Fr and boiling number Bo . The convection number Co represents the influence of the vapor quality; the Froude number Fr represents the ratio of inertia to gravity;

Fig. 13 Comparison of two-phase local Nu by experiment and new correlation



the definition of boiling number Bo represents the dimensionless heat flux, they are defined in Eq. (36), (37) and (38) respectively.

$$Co = \left(\frac{\rho_v}{\rho_l} \right) \left(\frac{1-x}{x} \right)^{0.8} \quad (36)$$

$$Fr = \frac{G^2}{\rho_l^2 g d_h} \quad (37)$$

$$Bo = \frac{\dot{q}}{G(h_v - h_l)} \quad (38)$$

By combining the calculation with Re_{eq} and Pr_l and considering these three parameters separately to check their contribution to Nu_{tp} , the correlation (Eq.39) was found to best match our experimental results.

$$Nu_{tp} = 29.327 Re_{eq}^{0.685} Pr_l^{1/3} Bo^{0.76} \quad (39)$$

Figure 13 reveals the comparison of the experimental results with the calculated results using the new correlation. The RMSE is approximately 10%, which is much smaller than other optimized correlations.

The waterside correlation is also obtained as shown in Eq. (40) using the method described above. Nevertheless, this correlation is only a suggestion due to the limitations of the experiment, in which the Reynolds number of cooling water changes within a small range ($2000 < Re_w < 3000$).

$$Nu_w = 5.189 Re_w^{0.202} Pr_w^{1/3} \quad (40)$$

5 Conclusion

An experimental investigation is carried out to study the two-phase local heat transfer of condensation in the PHE with micro-pits. The local temperatures of the water side and the wall are measured along the plate, and a calculation model is applied to determine the two-phase local heat transfer coefficient of R134a. The results are compared with the previous experimental work, which uses an unstructured PHE with the same geometric parameters under the same working conditions, and a new correlation is developed based on the available correlations in the literature.

- (1) The increase of mass flux leads to a significant improvement in the two-phase local heat transfer performance. The high saturation pressure has a positive effect on Nu_{tp} at the beginning of the condensation, but Nu_{tp} decreases with the increase of the saturation pressure in the later stage of condensation. The effect of the heat flux on the two-phase local heat transfer is not regular,

since these three factors interact with each other in the experiment.

- (2) Nu_{tp} increases as the vapor quality increasing in both micro-structured plates and unstructured plates. The enhancement of the two-phase local heat transfer for these two types of plates occurs at the entrance of the micro-structured PHE, where the condensate seems to be thinner.
- (3) Compared with the unstructured PHE, R134a in the micro-structured PHE condenses faster at the beginning of the condensation process, while the heat transfer performance is better in the areas with more liquid phase. Furthermore, the micro-structured plate could obtain a higher overall heat flux. Consequently, the micro-structured plate has better overall heat transfer performance, but only improves local heat transfer in low vapor quality areas.
- (4) A new correlation of two-phase local heat transfer for the micro-structured plate condenser is developed as shown in Eq. (39), which is compared with the experimental data and reaches a satisfactory agreement with a minimum RMSE of 10%. A new correlation for the water side is also recommended when the Re_w is ranged from 2000 to 3000.

Acknowledgements The author acknowledge the financial support from the China Scholarship Council (CSC) under contract No. 201708330250.

Authors' contributions All authors contributed to the study conception and design. Material preparation, data collection and analysis were performed by Ru Wang and Tingyan Sun. The first draft of the manuscript was written by Ru Wang and all authors commented on previous versions of the manuscript. All authors read and approved the final manuscript.

Funding Open Access funding enabled and organized by Projekt DEAL. The research is supported by China Scholarship Council (CSC) under contract No. 201708330250

Data availability Data are available on request to the authors.

Code availability The code used to support the findings of this study is custom code, which is available from the corresponding author upon request.

Declarations

Conflict of interests On behalf of all authors, the corresponding author states that there is no conflict of interest.

Open Access This article is licensed under a Creative Commons Attribution 4.0 International License, which permits use, sharing, adaptation, distribution and reproduction in any medium or format, as long as you give appropriate credit to the original author(s) and the source, provide a link to the Creative Commons licence, and indicate if changes were made. The images or other third party material in this article are included in the article's Creative Commons licence, unless indicated

otherwise in a credit line to the material. If material is not included in the article's Creative Commons licence and your intended use is not permitted by statutory regulation or exceeds the permitted use, you will need to obtain permission directly from the copyright holder. To view a copy of this licence, visit <http://creativecommons.org/licenses/by/4.0/>.

References

- Longo GA, Gasparella A, Sartori R (2004) Experimental heat transfer coefficients during refrigerant vaporisation and condensation inside herringbone-type plate heat exchangers with enhanced surfaces. *Int J Heat Mass Transf* 47(19–20):4125–4136. <https://doi.org/10.1016/j.ijheatmasstransfer.2004.05.001>
- Yan YY, Lio HC, Lin TF (1999) Condensation heat transfer and pressure drop of refrigerant R-134a in a plate heat exchanger. *Int J Heat Mass Transf* 42(6):993–1006. [https://doi.org/10.1016/S0017-9310\(98\)00217-8](https://doi.org/10.1016/S0017-9310(98)00217-8)
- Jokar A, Eckels S, Honsi MH, Giolda TP (2004) Condensation heat transfer and pressure drop of brazed plate heat exchangers using refrigerant R-134a. *J Enhanc Heat Transf*, 11(2). <https://doi.org/10.1615/JEnhHeatTransf.v11.i2.50>
- García-Cascales JR, Vera-García F, Corberán-Salvador JM, González-Maciá J (2007) Assessment of boiling and condensation heat transfer correlations in the modelling of plate heat exchangers. *Int J Refrig* 30(6):1029–1041. <https://doi.org/10.1016/j.ijrefrig.2007.01.004>
- Kuo WS, Lie YM, Hsieh YY, Lin TF (2005) Condensation heat transfer and pressure drop of refrigerant R-410A flow in a vertical plate heat exchanger. *Int J Heat Mass Transf* 48(25–26):5205–5220. <https://doi.org/10.1016/j.ijheatmasstransfer.2005.07.023>
- Han DH, Lee KJ, Kim YH (2003) The characteristics of condensation in brazed plate heat exchangers with different chevron angles. *J Korean Phys Soc* 43(1):66–73
- Thonon B, Bontemps A (2002) Condensation of pure and mixture of hydrocarbons in a compact heat exchanger: experiments and modelling. *Heat Transf Eng* 23(6):3–17. <https://doi.org/10.1080/01457630290098718>
- Shah MM (1979) A general correlation for heat transfer during film condensation inside pipes. *Int J Heat Mass Transf* 22(4):547–556. [https://doi.org/10.1016/0017-9310\(79\)90058-9](https://doi.org/10.1016/0017-9310(79)90058-9)
- Mancin S, Del Col D, Rossetto L (2012) Partial condensation of R407C and R410A refrigerants inside a plate heat exchanger. *Exp Therm Fluid Sci* 36:149–157. <https://doi.org/10.1016/j.expthermflusci.2011.09.007>
- Longo GA, Gasparella A (2007) Heat transfer and pressure drop during HFC-134a condensation inside a commercial brazed plate heat exchanger. In: *Proceeding of the International Congress of Refrigeration 2007, Beijing*, pp No. ICR07-B1–297
- Longo GA (2008) Refrigerant R134a condensation heat transfer and pressure drop inside a small brazed plate heat exchanger. *Int J Refrig* 31(5):780–789. <https://doi.org/10.1016/j.ijrefrig.2007.11.017>
- Longo GA (2009) R410A condensation inside a commercial brazed plate heat exchanger. *Exp Therm Fluid Sci* 33(2):284–291. <https://doi.org/10.1016/j.expthermflusci.2008.09.004>
- Longo GA (2010) Heat transfer and pressure drop during hydrocarbon refrigerant condensation inside a brazed plate heat exchanger. *Int J Refrig* 33(5):944–953. <https://doi.org/10.1016/j.ijrefrig.2010.02.007>
- Longo GA (2010) Heat transfer and pressure drop during HFC refrigerant saturated vapour condensation inside a brazed plate heat exchanger. *Int J Heat Mass Transf* 53(5–6):1079–1087. <https://doi.org/10.1016/j.ijheatmasstransfer.2009.11.003>
- Longo GA, Zilio C (2012) HFO1234yf condensation inside a brazed plate heat exchanger. In: *Proceeding of the 14th International Refrigeration and Air Conditioning Conference*, pp No. 1172
- Longo GA, Zilio C, Righetti G, Brown JS (2014) Condensation of the low GWP refrigerant HFO1234ze (E) inside a Brazed Plate Heat Exchanger. *Int J Refrig* 38:250–259. <https://doi.org/10.1016/j.ijrefrig.2013.08.013>
- Longo GA, Zilio C, Righetti G (2015) Condensation of the low GWP refrigerant HFC152a inside a Brazed Plate Heat Exchanger. *Exp Therm Fluid Sci* 68:509–515. <https://doi.org/10.1016/j.expthermflusci.2015.06.010>
- Wang L, Sundén B, Manglik RM (2007) *Plate heat exchangers: design, applications and performance* (Vol. 11). WIT Press, Boston
- Eldeeb R, Aute V, Radermacher R (2016) A survey of correlations for heat transfer and pressure drop for evaporation and condensation in plate heat exchangers. *Int J Refrig* 65:12–26. <https://doi.org/10.1016/j.ijrefrig.2015.11.013>
- Tao X, Ferreira CAI (2019) Heat transfer and frictional pressure drop during condensation in plate heat exchangers: Assessment of correlations and a new method. *Int J Heat Mass Transf* 135:996–1012. <https://doi.org/10.1016/j.ijheatmasstransfer.2019.01.132>
- Longo GA, Righetti G, Zilio C (2015) A new computational procedure for refrigerant condensation inside herringbone-type Brazed Plate Heat Exchangers. *Int J of Heat Mass Transf* 82:530–536. <https://doi.org/10.1016/j.ijheatmasstransfer.2014.11.032>
- Chu K H (2013) *Micro and nanostructured surfaces for enhanced phase change heat transfer*. Dissertation. Massachusetts Institute of Technology
- Nilpueng K, Wongwises S (2015) Experimental study of single-phase heat transfer and pressure drop inside a plate heat exchanger with a rough surface. *Exp Therm Fluid Sci* 68:268–275. <https://doi.org/10.1016/j.expthermflusci.2015.04.009>
- Polzin A-E (2020) *Evaporation and condensation in plate heat exchangers with microstructured surfaces*. Dissertation. Leibniz University Hannover
- Cassie ABD, Baxter S (1944) Wettability of porous surfaces. *Trans Faraday Soc* 40:546–551
- Bassiouny MK (1985) *Experimentelle und theoretische Untersuchungen über Mengen-stromverteilung, Druckverlust und Wärmeübergang in Plattenwärmetauschern*. Dissertation. Universität Heidelberg
- Collier JG, Thome JR (2004) *Convective boiling and condensation*. Clarendon Press, Oxford
- Martin H (1996) A theoretical approach to predict the performance of chevron-type plate heat exchangers. *Chem Eng Process: Process Intensification* 35(4):301–310. [https://doi.org/10.1016/0255-2701\(95\)04129-X](https://doi.org/10.1016/0255-2701(95)04129-X)
- Grabenstein V (2014) *Experimental investigation and modeling of condensation in plate heat exchangers*. Dissertation. Leibniz University Hannover
- Lockhart RW, Martinelli RC (1949) Proposed correlation of data for isothermal two-phase, two-component flow in pipes. *Chem Eng Prog* 45(1):39–48
- Moffat RJ (1988) Describing the uncertainties in experimental results. *Exp Thermal Fluid Sci* 1(1):3–17. [https://doi.org/10.1016/0894-1777\(88\)90043-X](https://doi.org/10.1016/0894-1777(88)90043-X)
- Würfel R, Ostrowski N (2004) Experimental investigations of heat transfer and pressure drop during the condensation process within plate heat exchangers of the herringbone-type. *Int J Therm Sci* 43(1):59–68. [https://doi.org/10.1016/S1290-0729\(03\)00099-1](https://doi.org/10.1016/S1290-0729(03)00099-1)
- Müller A, Polzin A-E, Kabelac S (2018) Multi-stream Plate-and-Frame Heat Exchangers for Condensation and Evaporation. In: *Bart HJ, Scholl S, Innovative Heat Exchangers*. Springer, Cham, pp 167–187. https://doi.org/10.1007/978-3-319-71641-1_5

Publisher's Note Springer Nature remains neutral with regard to jurisdictional claims in published maps and institutional affiliations.